Science & Nanotechnology
DOI: Article

Thouless energy in Josephson SN-N-NS bridges

S. V. Bakurskiy,[1,2] V. I. Ruzhickiy,[1,2] A. A. Neilo,[1] N. V. Klenov,[2,3] I. I. Soloviev,[1,2] A. A. Elistratova,[2,4] A. G. Shishkin,[2,4] V. S. Stolyarov[2,4] and M. Yu. Kupriyanov[1]

[1] *Skobeltsyn Institute of Nuclear Physics, Lomonosov Moscow State University, Moscow 119991, Russia*
[2] *Dukhov All-Russia Research Institute of Automatics, Moscow 101000, Russia*
[3] *Faculty of Physics, Lomonosov Moscow State University, Moscow 119992, Russia*
[4] *Center for Advanced Mesoscience and Nanotechnology, Moscow Institute of Physics and Technology, Dolgoprudny 141700, Russia*

submitted 9 February 2024, accepted 20 June 2024, published 27 July 2024

We have studied the Thouless energy in Josephson superconductor – normal metal – superconductor (SN-N-NS) bridges analytically and numerically, considering the influence of the sub-electrode regions. We have discovered a significant suppression of the Thouless energy with increasing interfacial resistance, consistent with experimental results. The analysis of the temperature dependence of the critical current in Josephson junctions in comparison with the expressions for the Thouless energy may allow the determination of the interface parameters of S and N-layers.

Introduction

In recent years, there has been a reawakened interest in Josephson structures in which the weak coupling region exhibits a metallic type of conductivity.[1–11] These structures are anticipated to surpass the integration limitations faced by superconducting devices used in digital information processing. The steady-state properties of SNS Josephson sandwiches and superconductor/normal metal/superconductor SN-N-NS bridges have been intensively studied.[10–19]

In Ref.[12] assuming the fulfillment of rigid boundary conditions at the SN interfaces, it was shown that in the case when the distance L between the S-electrodes significantly exceeds the characteristic decay length of superconducting correlations in the N-layer $\xi = (D/2\pi T)^{1/2}$, the decay of the critical current I_c with increasing L depends significantly on the ratio between the operating temperature T and the critical temperature of the superconducting electrodes T_c (here D is the diffusion coefficient of an ordinary metal). At small temperature ($T \ll T_c$) there is a power dependence ($I_c \propto 1/L^2$). With increasing temperature, the dependence of I_c on L becomes exponential: $I_c \propto \exp(-L/\xi)$.

In Ref.[17] these studies were complemented by a more detailed analysis of the temperature dependence of the critical current at low temperatures $T \ll T_c$. Numerical calculations carried out in Ref.[17] allowed the authors to propose an approximation formula for I_c

$$\frac{eI_cR_n}{E_T} = \alpha\left(1 - \beta\exp\left(-\frac{\alpha E_T}{3.2T}\right)\right), \quad E_T = \frac{D}{L^2}. \quad (1)$$

The fitting parameters $\alpha \approx 10.82$ and $\beta \approx 1/3$ correspond to the limit of small Thouless energy E_T as compared to the magnitude of the order parameter Δ in S-electrodes. In the opposite limit ($E_T \gg T$) the dependence $I_c(E_T)$ has the following form

$$\frac{eI_cR_n}{E_T} = \frac{32}{3+2\sqrt{2}}\left(\frac{2\pi T}{E_T}\right)^{3/2}\exp\left(-\sqrt{\frac{2\pi T}{E_T}}\right). \quad (2)$$

The publication of these results[17] stimulated the study of SNS-based structures aiming to experimentally determine the Thouless energy.[17,18,20–42] Experimental studies have shown that the values of the parameter α in the expression (1) obtained in Ref.[17] are at least several times larger than their experimental values. As a possible reason for this discrepancy, the presence of finite transparency of the SN boundaries of the studied Josephson contacts has been hypothesized. To account for this circumstance, a renormalization of the Thouless energy was proposed[18]

$$E_T^{\text{eff}} = E_T\frac{Ar^B}{C+r}, \quad \text{where} \quad r = \frac{G_N}{G_B}. \quad (3)$$

Here, r is normalization coefficient, G_N and G_B are the conductance of the normal wire and the SN interface, respectively, A, B, and C are fitting parameters. It is important to note that the authors of Ref.[18] "do not have a good explanation of the factor r^B and the numerical value of B" that they used to fit the data. Additionally, the fitting coefficients A, B, and C are not universal. Even for a set of samples differing by the distance L between the electrodes with fixed other parameters, all these coefficients will be sample-dependent.

It should be noted that almost all the experimental works cited above used the shadow mask technique to fabricate SNS-based Josephson contacts. The resulting hybrid structures had the SN-N-NS bridge geometry shown in figure 1. In this type of contact, the effective distance L_{eff} between the S-electrodes is not the geometric size L of the weak bonding region. This region is delocalized (in the other words, without rigid boundaries) and includes the areas of the N-film under the superconductors where current injection into the superconductor takes place. The presence of such delocalization was also qualitatively indicated by the experimental data. Indeed, substitution of the experimentally determined E_T into the expression (1) gave an estimate of the size of the weak coupling region, which is larger than L. In our opinion,

there is a significant difference in the geometry of the SN and SN-NS interfaces that leads to an overestimation of the theoretical value of the Thouless energy calculated using rigid boundary conditions at the interface of the composite SN electrode with the N-film of the bridge. The purpose of this article is to perform a detailed analysis of the proximity effect between the SN electrode and the N-film of SN-N-NS bridge structures and to derive an expression for the Thouless energy that takes into account both the finite transparency of their SN boundaries and the delocalization of the weak link region.

Before that, it is first necessary to define what we mean by the Thouless energy in Eq. (1) in the considered SN-N-NS structures. According to the definition[43–46] E_T characterizes the sensitivity of the energy state of the system to a modification of boundary conditions. This correlates with the existing characteristic scale of spatial changes in the system's parameters with its geometric dimensions. Unfortunately, for SN-N-NS junctions the geometric size of the weak link region cannot be strictly determined. Moreover, a supercurrent across the junction is expressed by the sum of the terms combined by the Green's function over the Matsubara frequencies, therefore the characteristic scale of spatial variations in the N-film $\xi_\omega = (D/2\omega)^{1/2}$ depends on the Matsubara frequencies $\omega = \pi T(2n+1)$, where $n = 0, 1, 2\ldots$ In the low-temperature range $T \ll T_c$ this sum converges at $\omega \approx \pi T_c$. Thus, there is wide range of parameters (L and ξ_ω) with some uncertainty in the choice of a single characteristic scale for spatial changes in the structure.

There is another interpretation of the Thouless energy. It suggests that two states whose energies differ by less than the Thouless energy are correlated. Otherwise, they can be considered as independent single-particle states whose energies are not shared. In our particular case, we are not dealing with the energy of states, but with a set of Green's functions which determine the supercurrent. The difference in the nature of the spatial changes in these functions is determined by the Matsubara frequency $\omega = \pi T(2n+1)$. Therefore, the interval at which the changes occur is equal to $2\pi T$.

In order to determine from a numerical solution of the Usadel equations or from experimental data the temperature T_{Th} for the transition from a sharp increase to a smooth character of the current change with decreasing temperature, we can introduce the Thouless energy for our problem as $E_T = 2\pi T_{Th}$. The Thouless energy determined in this way gives us the temperature at which the structural transitions from a discrete to an integral representation of its properties, such as the order parameter and the superconducting current (supercurrent), takes place.

It should be emphasized that the definition of $E_T = 2\pi T_{Th}$ is absolutely equivalent to the standard definition of E_{Th} in Eq. (1). By introducing the Thouless energy as described above, we can further use the relation (1) to estimate the characteristic scale of spatial variations in SNS structure as $L = (D/2\pi T_{Th})^{1/2} = \xi$ and thus find that L coincides with ξ_ω at the first Matsubara frequency $\omega = \pi T$ and $T = T_{Th} = E_T/2\pi$, that is, with the maximum value among the scales ξ_ω. In other words, the result of the above reasoning can be reformulated as follows: the Thouless energy is indeed defined by the expression (1). The value of the Thouless temperature $T_{Th} = E_T/2\pi$ required for processing of experimental data follows from the equality of the geometrical size of the structure with the maximum value of ξ_ω among the set of characteristic scales of the problem.

Thus, according to the established rule for the Thouless energy E_T in the considered planar SN-N-NS structures, we have to proceed from the equality of the scale ξ_ω to the effective geometric size of the weak coupling region $L + \zeta_\omega$

$$\xi_\omega = L + 2\kappa\zeta_\omega \tag{4}$$

at the first Matsubara frequency $\omega = E_T/2$. Here, ζ_ω is the maximum value among characteristic scales of spatial changes in the N-layer underneath the S-films and κ is a parameter that fixes the part of the effective coherence length ζ_ω by which the effective distance between the electrodes increases (formal definition of κ is given below). Note that at $\zeta_\omega = 0$ the expression (4) is transformed into the definition (1) of E_T, which was previously used to describe SNS sandwiches with rigid boundary conditions at the SN interfaces.

To determine ζ_ω it is sufficient to solve the problem on the proximity effect between a semi-infinite N-film and an extended SN electrode.

1 Proximity effect between extended SN electrode and semi-infinite N-film

We assume that the dirty-limit conditions are satisfied both in the superconductor and normal metal in the bridge, its SN boundaries have finite transparency, and the thickness of the N-film d_N is much less than $\xi_N = (D/2\pi T_c)^{1/2}$. The suppression of superconductivity in the S-film due to the proximity effect with the N-layer is considered negligible and it is not taken into account. Under these assumptions the proximity effect between the semi-infinite SN electrode (at $x \geq 0$) and the semi-infinite N-film (at $x \leq 0$) can be considered in the framework of the Usadel equations.[47] It was shown[48] that the Usadel equation for the θ function in the N-film under the S-electrode they can be written in the form

$$\zeta_\omega^2 \frac{\partial^2}{\partial x^2}\theta - \sin(\theta - \theta(\infty)) = 0, \; x \geq 0, \tag{5}$$

where

$$\theta(\infty) = \arctan \frac{\pi T_c \sin(\theta_S)}{\omega\gamma_{BM} + \pi T_c \cos(\theta_S)} \tag{6}$$

and

$$\cos(\theta_S) = \frac{\omega}{\sqrt{\omega^2 + \Delta^2}}, \; \sin(\theta_S) = \frac{\Delta}{\sqrt{\omega^2 + \Delta^2}}, \tag{7}$$

$\gamma_{BM} = \gamma_B d/\xi_N$, $\gamma_B = R_B/\rho_N\xi_N$, R_B is the specific boundary resistance, Δ is the absolute value of the order

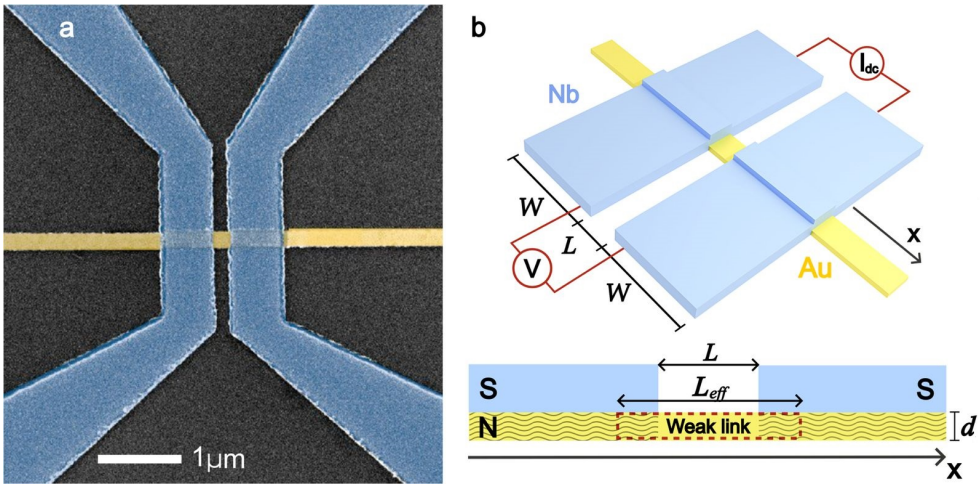

Figure 1. **a** – Scanning electron microscope image of an Nb/Au-Au-Au/Nb bridge with superconducting Nb electrodes and an Au weak link. **b** – Top part: three-dimensional sketch of the Josephson superconductor/normal metal/superconductor (SN-N-NS) bridge. The sample is connected using a four-point scheme. Bottom part: side view of the Josephson SN-N-NS bridge. Wavy lines indicate the proximized region of the N-layer under the S-electrode, and the red frame indicates the effective weak link.

parameter in the S layer, which has the BCS-like temperature dependence. We conclude that

$$\frac{\zeta_\omega}{\xi_\omega} = \sqrt{\frac{\omega\gamma_{BM}}{\sqrt{(\omega\gamma_{BM})^2 + 2\pi T_c\omega\gamma_{BM}\cos(\theta_S) + (\pi T_c)^2}}}. \quad (8)$$

The Usadel equation in the N-film can be written as follows

$$\xi_\omega^2\frac{\partial^2}{\partial x^2}\theta - \sin\theta = 0, \quad x \le 0. \quad (9)$$

The existence of the first integrals of the equations (5) and (9)

$$\zeta_\omega\frac{\partial}{\partial x}\theta = 2\sin\left(\frac{\theta(\infty)-\theta}{2}\right), \quad x \ge 0, \quad (10)$$

$$\xi_\omega\frac{\partial}{\partial x}\theta = 2\sin\frac{\theta}{2}, \quad x \le 0, \quad (11)$$

permits to get their analytical solutions

$$\theta = \theta(\infty) + 4\arctan\left[Q\exp\left(-\frac{x}{\zeta_\omega}\right)\right], \quad x \ge 0, \quad (12)$$

$$\theta = 4\arctan\left[\left(\tan\frac{\theta(-0)}{4}\right)\exp\left(\frac{x}{\xi_\omega}\right)\right], \quad x \le 0, \quad (13)$$

where

$$Q = \tan\frac{\theta(+0)-\theta(\infty)}{4}.$$

The integration constants $\theta(\pm 0)$ in Eqs. (12)–(13)

$$\theta(\pm 0) = 2\arctan\frac{\sin\frac{\theta(\infty)}{2}}{\cos\frac{\theta(\infty)}{2}+g}, \quad g = \frac{\xi_\omega}{\zeta_\omega}. \quad (14)$$

have been determined from the boundary conditions

$$\frac{\partial}{\partial x}\theta(+0) = \frac{\partial}{\partial x}\theta(-0) \quad \text{and} \quad \theta(+0) = \theta(-0) \quad (15)$$

at SN-N interface ($x = 0$).

2 Thouless energy

Substitution of Eq. (8) into Eq. (4) at the first Matsubara frequency $\omega = E_T/2$ results in

$$\frac{L}{\xi_N} + 2\kappa\sqrt{\frac{\gamma_{BM}}{\sqrt{\epsilon^2\left(\gamma_{BM}^2 + 2\gamma^*\gamma_{BM}\right)+1}}} = \sqrt{\frac{1}{\epsilon}}, \quad (16)$$

where $\epsilon = E_T/2\pi T_c$, $\gamma^* \approx 1.781$ is Euler's constant. For simplicity we replace Δ with its value $\pi T_c/\gamma^*$ at $T \ll T_c$.

In the limit $\epsilon\gamma_{BM} \gg 1$ Eq. (16) transforms to

$$\epsilon = \frac{\xi_N^2}{L^2}\left(1 - 2\kappa\sqrt{\frac{\gamma_{BM}}{\sqrt{\gamma_{BM}^2 + 2\gamma^*\gamma_{BM}}}}\right)^2. \quad (17)$$

Note that as $\gamma_{BM} \to \infty$ the SN boundaries become completely non-transparent for quasiparticles in the N-region, therefore thequasiparticle current cannot flow from the N-film of the SNS contact into the S-electrodes. If the length of the SN boundaries of the composite SN electrodes of the SN-N-NS structure significantly exceeds ζ_ω, the length of the current localization region in its N-part can be considered infinite. Therefore, in full agreement with Eq. (1), the parameter ϵ should tends to zero, as $\gamma_{BM} \to \infty$. From this requirement we get $\kappa = 1/2$ and

$$\epsilon = \frac{\xi_N^2}{L^2}\left(1 - \sqrt{\frac{\gamma_{BM}}{\sqrt{\gamma_{BM}^2 + 2\gamma^*\gamma_{BM}}}}\right)^2. \quad (18)$$

Suppose further that the parameter κ is independent on γ_{BM} in the opposite limit $\epsilon\gamma_{BM} \ll 1$, then we get

$$\epsilon = \frac{\xi_N^2}{(L + \xi_N\sqrt{\gamma_{BM}})^2}. \quad (19)$$

Figures 2a,b show the dependence of the Thouless energy E_T on the suppression parameter γ_{BM}, calculated using equations (16), (17), and (19), for the distances between the electrodes SN-N-NS structures, which are

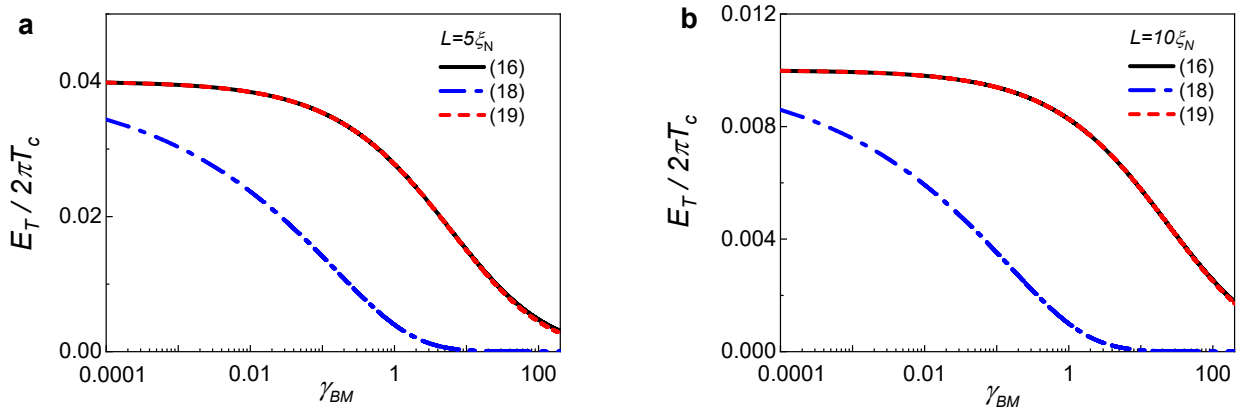

Figure 2. **a**, **b** – Thouless energy E_T versus interface parameter γ_{BM} in the SN-N-NS bridge with the distances between the electrodes $L = 5\xi_N$ (panel a) and $L = 10\xi_N$ (panel b), calculated from the Eq. (16) (solid line) and from the asymptotic expressions (18) (dash-dotted line) and (19) (dashed line), valid in the limit of $\epsilon\gamma_{BM} \gg 1$ and $\epsilon\gamma_{BM} \ll 1$, respectively.

$L = 5\xi_N$ and $L = 10\xi_N$. The calculations show that the approximation formula (19) coincides with the exact dependence $E_T(\gamma_{BM})$ calculated by the formula (16) within the specified range of parameters for long bridges. A noticeable discrepancy between the curves calculated by formulas (16) and (19) only appears in the $\gamma_{BM} \gg 100$ limit – this scenario is not realized in the experiments involving SN-N-NS structures.

At the same time, the expression (17) fits the exact dependency $E_T(\gamma_{BM})$ rather poorly. The reason is that the condition $\epsilon\gamma_{BM} \gg 1$ is not fulfilled even in the region of large γ_{BM}. This is due to the fact that ϵ decreases much faster than γ_{BM}^{-1}. The difference between the exact solution (16) and that resulting from asymptotic expression (17) becomes more obvious as L/ξ_N increases.

It is easy to see that when $L \gg \xi_N\sqrt{\gamma_{BM}}$ the expression (16) is reduced to Eq. (1). Physically, this limit is equivalent to the fulfillment of rigid boundary conditions at the N boundaries of the bridging film with its NS electrodes. In this limit, as in the SNS sandwiches investigated in Ref.[17] the rigid boundary conditions do not impose any additional characteristic lengths characterizing the spatial variations of parameters in the N film of SNS or SN-N-NS structures. The weak coupling region turns out to be a "closed" system, characterized only by its intrinsic parameters, such as the diffusion coefficient D. The Thouless energy (1) was introduced precisely for such "closed" systems.

Going beyond the rigid boundary conditions, such as considering the finite transparency of SN boundaries in SNS sandwiches or the delocalization of the weak coupling region in the studied SN-N-NS structures, violates the closure condition. Additional scales appear in the problems determined by the suppression parameter γ_B in SNS sandwiches or γ_{BM} in SN-N-NS structures. Therefore, in SN-N-NS bridges in accordance with the formula (16) at $L \ll \xi_N\sqrt{\gamma_{BM}}$ the diffusion coefficient no longer characterizes the system and the Thouless energy $E_T = \pi T_c/\gamma_{BM}$ in the first approximation is determined only by the parameter γ_{BM}, *i.e.*, by the properties of the SN boundaries.

The proposed implicit definition (16) of E_T is a compromise solution, considering both the internal parameters of the N-metal in the weak coupling region and the peculiarities of induced superconducting correlations in in the N-metal.

3 Calculation of a supercurrent across SN-N-NS junction

The dependence of the superconducting current density I on the phase difference of the order parameters of the superconducting electrodes φ in the SN-N-NS junctions has been previously calculated by numerically in Ref.[10] for arbitrary values of γ_{BM} and L/ξ_N. Just as in the approach we used earlier in Section II, the suppression of superconductivity in the S-film was not taken into account in Ref.[9] For computational convenience, the Usadel equations were written in the Φ representation (the origin of the $0x$ axis is placed in the center of the structure)

$$\xi_{\rm eff}^2 \frac{\partial}{\partial x}\left(G^2\frac{\partial\Phi}{\partial x}\right) - \Phi = -\delta, \quad x \geq L/2; \tag{20}$$

$$\frac{\partial}{\partial x}\left(G^2\frac{\partial\Phi}{\partial x}\right) - \Omega G\Phi = 0, \quad 0 \leq x \leq L/2; \tag{21}$$

$$\xi_{\rm eff}^2 = \frac{\gamma_{BM}}{G\,(G_s + \gamma_{BM}\Omega)}, \quad \delta = \frac{G_s\Delta\exp(i\varphi/2)}{(G_s + \gamma_{BM}\Omega)}; \tag{22}$$

$$\frac{I}{I_0} = \frac{2\pi T}{T_c}\sum_{\Omega\geq 0}^{\infty}\frac{G^2}{\Omega^2}\left(\mathrm{Im}\,\Phi\,\frac{\partial\,\mathrm{Re}\,\Phi}{\partial x} - \mathrm{Re}\,\Phi\,\frac{\partial\,\mathrm{Im}\,\Phi}{\partial x}\right). \tag{23}$$

Here, Φ and $G = \Omega/(\Omega^2 + \Phi\Phi^*)^{1/2}$ are Usadel Green's functions, the Matsubara frequencies $\Omega = (2n+1)T/T_c$ are normalized on πT_c, the x-coordinate is normalized on ξ_N, and $I_0 = T_c/e\xi_n\rho_N$, where ρ_N is residual resistivity of the N-film. The modulus of the order parameter in the S-electrode Δ has the BCS-like temperature dependence

and it is normalized on πT_c; $\varphi/2$ is the phase of the order parameter for the right electrode ($x \gtrsim L/2$).

Equations (20) and (21) should be supplemented by appropriate boundary conditions. At $x = 0$ these conditions follow from the symmetry of the considered problem

$$\frac{\partial \operatorname{Re}\Phi}{\partial x} = 0 \quad \text{and} \quad \operatorname{Im}\Phi = 0. \tag{24}$$

At a large distance from the N-NS boundary, the function Φ converges to a solution that is independent of x

$$\Phi = \delta. \tag{25}$$

Figures 3a,b show the $I_c(T)$ dependences calculated for $L = 5\xi_N$ and for various interface parameters γ_{BM} ranging from 0.01 to 100. For convenience, they are presented in linear and logarithmic scales. The points on these curves ($\circ$) correspond to the halfed Thouless energy ($T/T_c = E_T/2$). The E_T values are calculated for $L = 5\xi_N$ and various γ_{BM} using Eq. (19). These figures clearly show that in the vicinity of $E_T/2$ the slope of the dependences $I_c(T)$ changes, *i.e.*, there is a transition from a smooth to a sharp temperature drop of $I_c(T)$ with increasing temperature (see figures 3a,b).

In addition to the temperature $T = E_T/2$, two other characteristic temperature values can be noted. They are $T = T_{Th} = E_T/2\pi$ marked with squares and $T = E_T$ marked with triangles on the temperature dependences of the first derivative of the critical current with respect to temperature (see figures 3c-f). Figures 3d,f clearly show that for $L = 5\xi_N$ and $\gamma_{BM} = 0.01$ the Thouless temperature is $T_{Th} \approx 0.04T_c$. The increase of the parameter γ_{BM} is accompanied by a shift of the values of this temperature towards $T = 0$, so that at $\gamma_{BM} = 2$, the value of T_{Th} turns out to be equal to $\approx 0.025T_c$. At $T = T_{Th}$ and below the critical current reaches saturation. So the first derivative dI_c/dT is zero at $T \lesssim T_{Th}$. From the presented in figures 3d,f dependences it also follows that there are two extra points to be mentioned. At $T \approx E_T$ and $\gamma_{BM} < 5$ the local minimum of the derivative is reached. At $T \approx E_T/2$ an inflection point of dI_c/dT appears for $\gamma_{BM} < 5$. Qualitatively, this point corresponds to the transition area between the saturation region and decreasing part of $I_c(T)$ dependence. These reference points at $T = E_T/2$ and $T = E_T$ can be useful when values of $T = T_{Th}$ are difficult to achieve due to limitations on the temperature range allowed for measurements. In the limit $\gamma_{BM} \gg 5$ the effective impact of boundaries increases and the positions of the considered points $T \approx E_T/2$ and $T \approx E_T$ are shifted.

Note that in the limit of a small critical current the boundary value problem (20)-(25) may also have an analytical solution. This limit is realized in the case when it is possible to neglect the suppression of anomalous Green's functions induced in the N-film by the current flowing through it.

4 Critical current of the long SN-N-NS bridge

In the $L \gg \xi$ limit, the superconducting state near the center of the bridge can be described by the superposition of anomalous Green's functions (13)–(14) penetrating from the superconducting banks into the bridge (see Refs.[16,49,50])

$$\frac{\Phi}{\omega} = \tan\left[\theta\left(-x - \frac{L}{2}\right)\right] e^{-i\frac{\varphi}{2}} + \tan\left[\theta\left(x - \frac{L}{2}\right)\right] e^{i\frac{\varphi}{2}}, \tag{26}$$

where $\theta(x)$ is the solutions of the proximity problem (12)–(14). By substituting this solution of the Usadel equations into the expression for the supercurrent [see Eq. (23)], we arrived at a sinusoidal dependence of the supercurrent on the phase difference φ with a critical current density equals to

$$\frac{I_c}{I_0} = \frac{128\pi T}{T_c} \sum_{\omega} \tan^2\left(\frac{1}{2}\arctan\frac{\sin\frac{\theta(\infty)}{2}}{\cos\frac{\theta(\infty)}{2} + g}\right) e^{-\frac{L}{\xi_\omega}}. \tag{27}$$

In the considered approximation ($L \gg \xi$) the critical current value is determined by the first term in the sum in Eq. (27):

$$\frac{I_c}{I_0} = \frac{128\pi T}{T_c} \tan^2\left(\frac{1}{2}\arctan\frac{\sin\frac{\theta(\infty)}{2}}{\cos\frac{\theta(\infty)}{2} + g}\right) e^{-\frac{L}{\xi}}, \tag{28}$$

where $\theta(\infty)$ is determined by Eq. (6) with $n = 0$, that is $\omega = \pi T$. The expression (28) is an analog of the formula (2) derived in Ref.[16] for SNS structures with rigid boundary conditions at the SN boundaries. Unlike from Eq. (2), the expression (28) takes into account both the finite transparency of the SN boundaries and the delocalization of the weak-link region.

Note that the expression (27) is also valid in the limit of large $\gamma_{BM} \gg 1$, if the distance L between the SN electrode is not too small, so that the sum in Eq. (27) converges at

$$\omega \lesssim \frac{\pi T_c}{\gamma_{BM}} \max\left[1, \frac{L}{\xi_N}\right]. \tag{29}$$

5 Comparison with experimental data

Theoretical results given above explain how T_{Th} can be determined on the basis of the available (calculated or experimentally obtained) $I_c(T)$ dependence. Then using the formula (19) one can find such an important parameter for practical applications as the effective geometric size of the SN-N-NS Josephson contacts

$$L_{\text{eff}} = L + \xi_N\sqrt{\gamma_{BM}}. \tag{30}$$

Note that Eq. (30) is a direct consequence of Eq. (19) and is valid up to $\gamma_{BM} \approx 100$, as it can be observed from the comparison of the exact (16) and asymptotic (19) solutions for E_T in figure 2.

Our experimental study of a supercurrent transport across Nb/Cu-Cu-Cu/Nb[34] and Nb/Au-Au-Au/Nb[39,41] bridges has shown that the shape of the exponentially-decreasing dependences of $I_c(T)$ in a wide temperature

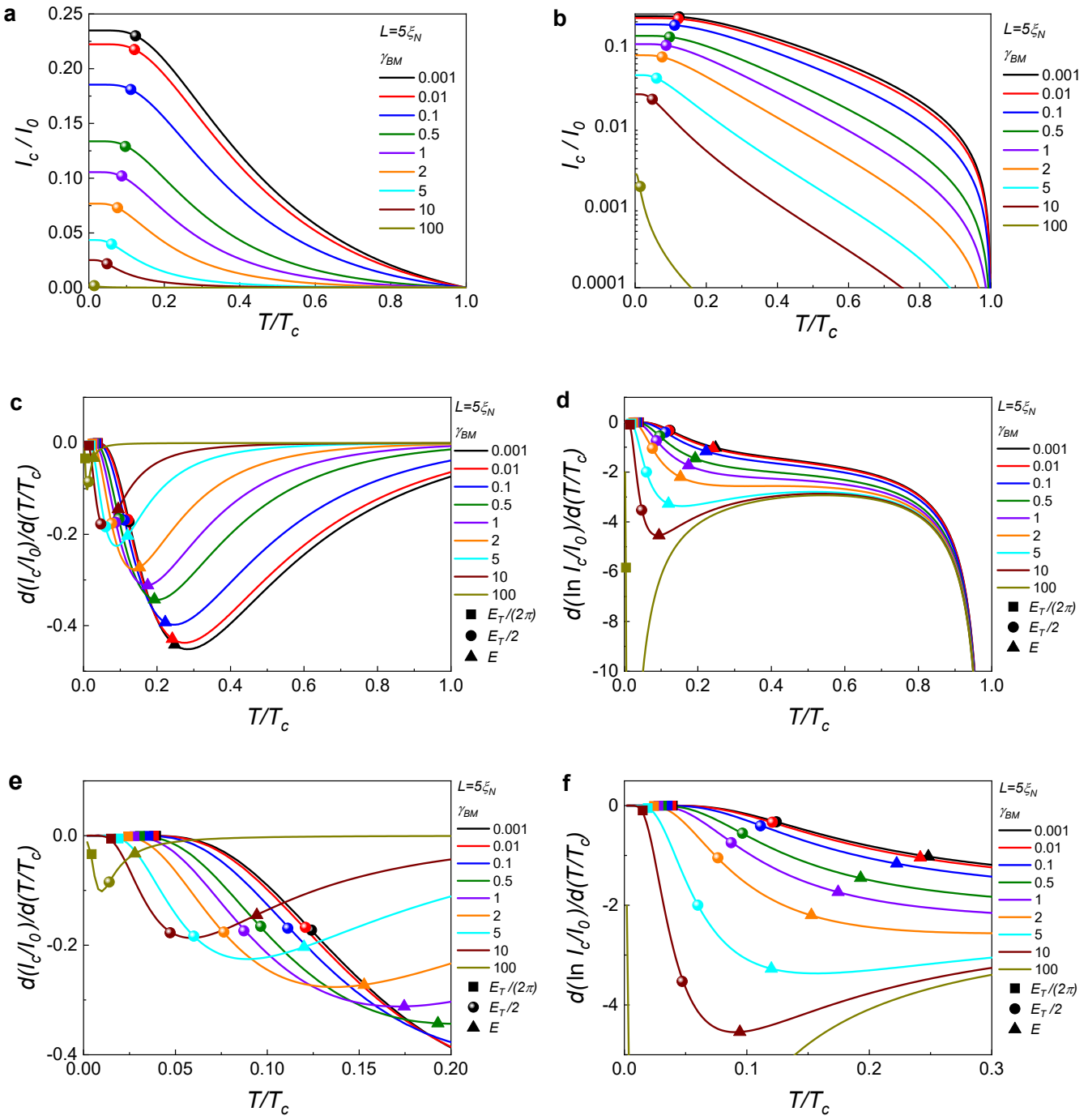

Figure 3. **a**, **b** – Temperature dependences of the critical current density I_c of the SN-N-NS bridge with $L = 5\xi$ calculated numerically for different interface parameters γ_{BM} in linear (panel a) and logarithmic (panel b) scales. **c-f** – Temperature dependences of the first derivative of the critical current density $\frac{dI_c/I_0}{dT/T_c}$ for the same parameters in linear (panel c) and logarithmic (panel d) scales, respectively. The squares, points, and triangles on each of the calculated curves show the temperature values corresponding to $E_T/(2\pi)$, $E_T/2$, and E_T, respectively. The values of E_T were calculated using the expression (19) for each combination of γ_{BM} and ξ_N parameters. Panels e and f are enlarged versions of panels c and d in the low-temperature region.

range closely resembles that shown in figure 3. At $\gamma_{BM} \lesssim 5$ and large values of $L \gtrsim 4\xi_N$ there is the transition at $T \approx T_c(\xi_N/L)^2$ from a sharp rise of $I_c(T)$ to a smoother saturation at $T \ll T_c$ as temperature decreases. At $\gamma_{BM} \gtrsim 5$ and small values of $L \lesssim 4\xi_N$ the change in the slope of the $I_c(T)$ dependence takes place at $T \approx T_c/\gamma_{BM}$.

In figure 4a we show the most recent experimental data for the Nb/Au-Au-Au/Nb Josephson bridge with a diffusive Au stripe operating as weak link. This structure was fabricated by magnetron sputtering and lift-off lithography. Further information concerning the fabrication process can be found in Refs.[39,41,51] The approximate distance between the SN electrodes can be estimated as $L \approx 160$ nm based on the scanning electron microscopy (see figure 1b). The thicknesses of niobium and gold layers are equal approximately 70 nm and 32 nm,

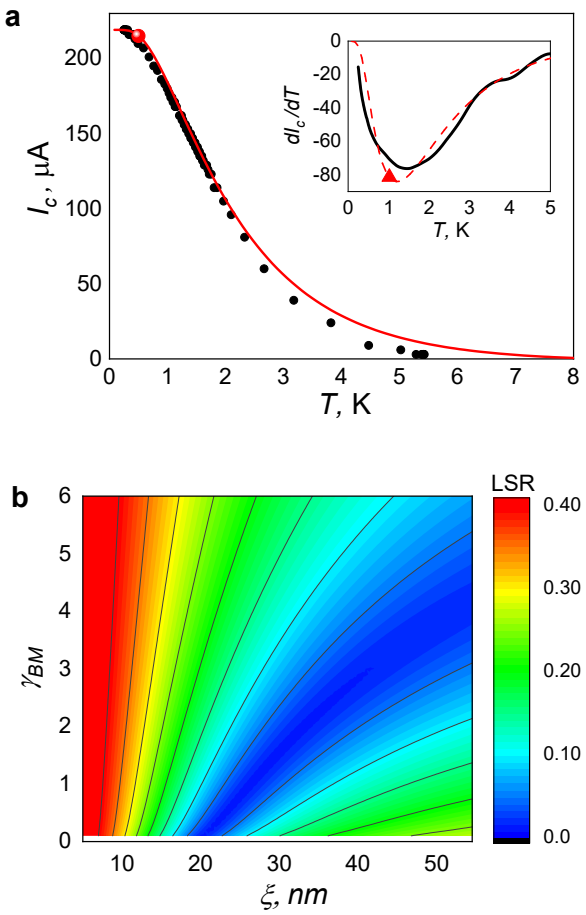

Figure 4. **a** – Temperature dependence of the critical current $I_c(T)$ for the NbAu-Au-AuNb bridge with the length of the weak link $L = 160$ nm (black circles) and numerical fits in the framework of the model (20)-(25) calculated at $\xi_N = 23$ nm and $\gamma_{BM} = 0.12$ (red line). The red dot marks the temperatures corresponding to the halfed Thouless energy $E_T/2$. The inset shows the derivative $dI_c(T)/dT$ of the interpolated experimental (black solid line) and model (red dashed line) $I_c(T)$ dependencies. **b** – The least-squares residual between the experimental data and the model fits in the $\gamma_{BM} - \xi$ plane of the parameters.

respectively.

To compare the experimental data presented in figure 4a with the results of the theoretical calculations, we construct a map which shows the dependence of the standard deviation between the experimental data and calculated dependence. The least-squares calculation of the standard deviation of the theoretical values of the critical current from the experimentally obtained points is shown in figure 4b. This procedure results in a detection of a valley on the $\gamma_{BM} - \xi$ diagram where the experimental points agree quite well with the theoretical calculation. It can be seen that the presence of two free parameters γ_{BM} and ξ does not lead to unique fitted solution. For different sets of γ_{BM} and ξ the formula (19) gives different E_T values.

It should be noted that for the considered case the expression (19) allows us to specify the range of parameters in which it is worthwhile to search for a solution of the system at sufficiently large effective bridge lengths $L \gtrsim 5\xi$ and transparent interfaces $\gamma_{BM} \lesssim 1$. As an example, in figure 4a we have shown one of possible approximation of the experimental dependence $I_c(T)$ with the solution of the Usadel equations obtained for $\xi_N = 23$ nm ($L/\xi_N \approx 7$) and $\gamma_{BM} = 0.12$ (red line). A large red dot on this graph marks the temperature $T \approx 0.5$ K, which corresponds to $E_T/2$ [see Eq. (19)]. The inset in figure 4a shows the derivative of the theoretical dI_c/dT dependence (red dashed line) and the interpolation curve obtained for the experimental points. The red triangle also marks the point where the temperature $T \approx 1$K coincides with the value corresponding to E_T. It is located near the minimum of the derivative dI_c/dT.

It should be emphasized that according to Eq. (30) for $L/\xi_N \approx 7$ and $\gamma_{BM} = 0.12$ the effective size of the structure $L_{\text{eff}} \approx 7.3\xi_N$ is actually determined by the distance between the electrodes L. In this case, the features of the shape of the dependence $I_c(T)$ are due to the transition from exponential to power laws of growth of I_c with decreasing temperature. As it can be illustrated in figure 3, the position of these features correlates quite well with T_{Th}. For shorter bridges ($L \lesssim 3\xi$) the $I_c(T)$ dependences are smoother and the bending of the curves $dI_c(T)/dT$ at $T = E_T/2$ are not as clear as for large L values. Also, in these case the interface parameter γ_{BM} increases resulting in a change of the shape of the $I_c(T)$ dependence.

Thus, we have shown that the expression (19) can be used to determine the range of parameters in which the optimal approximation of the experimental results should be sought. For a more unambiguous extraction of the structural parameters from the experimental dependence $I_c(T)$, it is necessary to approximate several samples simultaneously with different lengths between the electrodes L, as done in Refs.[34,41] and use additional data ρ_n and γ_B extracted from the temperature dependence of the normal-state resistance at $T > T_c$. This approach allows one to significantly reduce the range of parameters for the best fitting by the microscopic model. However, it requires a complete construction of the parameter map, which is a rather time-consuming.

We demonstrate that the theoretical curve fits the experimental data well at $T \lesssim 4$ K. The observed discrepancy between the theoretical predictions and the experimental data at higher temperatures ($T \gtrsim 4$ K) may be due to the following reasons.

Possible difference in the critical temperature of the region of the S layer adjacent to the N-film T_{cl} compared to the measured T_c of the bulk S electrode, as well as coordinate dependence of T_{cl}. Another factor could be an inhomogeneity of the transparency of the NS boundaries, caused both by mechanical stresses at the NS interfaces, and their roughness. All these factors lead to the appearance of inhomogeneous island-type superconductivity in the N-layer which is more pronounced at $T \to T_c$, *i.e.*, to the appearance of the dependence $\delta(x)$ in Eq. (22), which was not considered in the developed theory.

It should be noted that such a successful coincidence of the Thouless energy values found from the numerically calculated dependences $I_c(T)$ and ones based on expression (19) does not mean that the E_T values determined

from the shape of the experimental curves $I_c(T)$ will lead to the same L_{eff} value determined by Eq. (30). A deviation of the experimentally determined L_{eff} value and the effective length defined by Eq. (30) may be due to the fact that some constrains controlling the applicability of the considered one-dimensional SN-N-NS contact are not realized experimentally.

Such restrictions include:

1. The smallness of the N-layer thickness compared to the decay length ξ_N. When using low-resistivity normal metals (Al, Au, Ag), the closeness of d to ξ_N can lead partial suppression of superconductivity in the S-layer near the SN boundary.[52,53]

$$\frac{d}{\xi_N}\frac{\rho_S}{\rho_N}\frac{\xi_S}{\xi_N} \lesssim 0.3, \tag{31}$$

where ρ_S and ξ_S are normal-state resistivity and coherence length of the S-film. Going beyond the one-dimensional approximation, the temperature T_{Th} actually decreases as d increases.[54] This automatically leads to an increase in the effective size of the SN-N-NS structure with respect to the L_{eff} value defined by expression (30).

2. The boundary condition (25) states that the current flowing through the N-layer of the SN composite electrode is negligible compared to the current that has entered the S-layer of the electrode, i.e.

$$\frac{d}{d_S}\frac{\rho_S}{\rho_N} \ll (1+\gamma_{BM})^2, \tag{32}$$

where d_S is the thickness of the S-film. A violation of this constraint should lead to the appearance of the dependence of the phase difference φ on the x-coordinate (see also the discussion in point 4 below).

3. At any point of the SN boundary, the density of the supercurrent injected from the normal metal through this interface into the S-layer should be less than the critical current density controlled by the finite transparency of this boundary, *i. e.*

$$1+\gamma_{BM}^{-1} > \frac{d}{\zeta}\max\left[\frac{\xi_N}{L}, 1\right]. \tag{33}$$

4. The final constrain arises from the assumption that the phase difference φ appearing in Eqs. (20) and (22) is independent of the x-coordinate. This assumption is valid for $x \gg L/2$. Away from the N-NS boundary, the superconducting current is uniformly distributed across the thickness of the NS electrode. The current flows along the $0x$ direction, so the current lines do not cross the NS boundary. As a result, at $x \gg L/2$ the phase of the order parameter in each cross sections of the NS electrode turns out to be equal to the phase of the anomalous Green's functions in both N and S-layers, and the $\varphi(x)$ function turns out to be a value independent of x (see Ref.[11] for details).

Conclusion

Thus, through analytical evaluations and numerical calculations, we have shown that the Thouless energy in Josephson SN-N-NS bridges strongly depends on the resistance of the SN interface. The Thouless energy decreases by several times as this resistance increases compared to the SNS sandwich-type contact. We have also specified the range of validity of our analytical results, thus providing the possible explanations for the deviation of the experimentally obtained L_{eff} from our analytical result (30).

The Thouless energy cannot be measured directly. Instead, the Thouless temperature can be determined by analyzing the shape characteristics of experimentally obtained $I_c(T)$ dependences. Thouless temperature can be defined as the temperature corresponding to the saturation of the $I_c(T)$ dependence at low temperatures and vanishing of the first derivative dI_c/dT. The use of this method for the experimental determination of T_{Th} requires measurements at rather low temperatures, which causes additional difficulties in finding T_{Th}. We have shown that the transition from the study of the dependence $I_c(T)$ to the determination of peculiar points on the temperature dependences of $dI_c(T)/dT$ located at $T \approx E_T/2$ and $T \approx E_T$ allows us to estimate the E_T value in the range of temperatures more convenient for measurements.

Our numerical calculations carried out in the framework of the one-dimensional SN-N-NS model of the Josephson SN-N-NS structure have shown that there is a relationship between the value of the Thouless energy $E_T = 2\pi T_{Th}$ determined in this way and the effective geometrical size of the structure L_{eff} [see Eq. (30)] included in formula (19). The estimate of L_{eff} obtained in this way is important in determining the limitations to miniaturization of the size of superconductor devices for processing analog and digital signals. It also provides additional information on the relationship between important technological parameters such as the NS electrode spacing L, decay length ξ_N, and the parameter γ_{BM}, which characterizes the transparency of NS boundaries.

Acknowledgements

We are grateful to A. I. Zaikin and A. A. Golubov for the discussion of the results obtained. A.N. thanks the support of the Foundation for the Development of Theoretical Physics and Mathematics "BASIS". The authors are grateful to MIPT Collective Use Center for providing facilities for samples fabrication. The experiments were carried out with the support of the Russian Science Foundation, Grant No. 23-72-30004.

Contact information

Corresponding author: Sergey V. Bakurskiy, orcid.org/0000-0002-6010-6697, e-mail r3zz@mail.ru.

Competing Interests

The authors declare no competing financial or non-financial interests.

References

[1] Kupriyanov M. Y., Brinkman A., Golubov A. A., Siegel M., Rogalla H. *Double-barrier Josephson structures as the novel elements for superconducting large-scale integrated circuits*. Physica C, vol. **326**, 16-45 (1999).

[2] Holmes D. S., Ripple A. L., Manheimer M. A. *Energy-Efficient Superconducting Computing-Power Budgets and Requirements*. IEEE Trans. Appl. Supercond, vol. **23**, 1701610 (2013).

[3] Shelly C. D, See P., Ireland J., Romans E. J., Williams, J. M. *Weak link nanobridges as single flux quantum elements*. Supercond. Sci. Technol., vol. **30**, 095013 (2017).

[4] Tolpygo S. K. *Superconductor Digital Electronics: Scalability and Energy Efficiency Issues*. Low Temp. Phys., vol. **42**, 361-379 (2016).

[5] Semenov V. K., Polyakov Y. A., Tolpygo S. K. *Very large scale integration of Josephson-junction-based superconductor random access memories*. IEEE Trans. Appl. Supercond, vol. **29**, 1302809 (2019).

[6] Collins J. A., Rose C. S., Casaburi A. *Superconducting Nb Nanobridges for Reduced Footprint and Efficient Next-Generation Electronics*. IEEE Trans. Appl. Supercond, vol. **33**, 1800208 (2023).

[7] Thompson M. L., Castellanos-Beltran M., Hopkins P. F., Dresselhaus P. D.; Benz S. P. *Effects of Nonsinusoidal Current Phase Relationships on Single Flux Quantum Circuits*. IEEE Trans. Appl. Supercond, vol. **33**, 1300205 (2022).

[8] Tolpygo S. K., Rastogi R., Weir T., Golden E. B., Bolkhovsky V. *Development of Self-Shunted Josephson Junctions For a Ten-Superconductor-Layer Fabrication Process: $Nb/NbN_x/Nb$ Junctions*. arXiv preprint:2312.13475 (2023).

[9] Tolpygo S. K., Rastogi R., Weir T., Golden E. B., Bolkhovsky V. *Development of Self-Shunted Josephson Junctions for a Ten-Superconductor-Layer Fabrication Process: $Nb/NbN_x/Nb$ Junctions*. IEEE Trans. Appl. Supercond, vol. **34**, 1101008 (2024).

[10] Soloviev I. I., Bakurskiy S. V., Ruzhickiy V. I., Klenov N. V., Kupriyanov M. Yu., Golubov A. A., Skryabina O. V., Stolyarov V. S. *Miniaturization of Josephson junctions for digital superconducting circuits*. Phys. Rev. Appl., vol. **16**, 044060 (2021).

[11] Ruzhickiy V., Bakurskiy S., Kupriyanov M., Klenov N., Soloviev I., Stolyarov V., Golubov A. *Contribution of Processes in SN Electrodes to the Transport Properties of SN-N-NS Josephson Junctions*. Nanomaterials, vol. **13**, 1873 (2023).

[12] Likharev K. K. *Superconducting weak links*. Rev. Mod. Phys., vol. **51**, 101 (1979).

[13] Golubov A. A., Kupriyanov M. Yu., Il'ichev E. *The current-phase relation in Josephson junctions*. Rev. Mod. Phys., vol. **76**, 411 (2004).

[14] Likharev K. K. Sov. Tech. Phys. Lett., vol. **2**, 12-13 (1976).

[15] Ivanov Z. G., Kupriyanov M. Y., Likharev K. K., Meriakri S. V., Snigirev, O. V. *Boundary-conditions for the Usadel and Eilenberger equations, and properties of dirty SNS sandwich-type junctions*. Sov. J. Low. Temp. Phys., vol. **7**, 274-281 (1981).

[16] Zaikin A., Zharkov G. Sov. J. Low Temp. Phys., vol. **7**, 184-185 (1981).

[17] Dubos P., Courtois H., Pannetier B., Wilhelm F. K., Zaikin A. D., Schön G. *Josephson critical current in a long mesoscopic SNS junction*. Phys. Rev. B, vol. **63**, 064502 (2001).

[18] Hammer J. C., Cuevas J. C., Bergeret F. S., Belzig, W. *Density of states and supercurrent in diffusive SNS junctions: Roles of nonideal interfaces and spin-flip scattering*. Phys. Rev. B, vol. **76**, 064514 (2007).

[19] Marychev P. M., Vodolazov D. Yu. *A Josephson junction based on a highly disordered superconductor/low-resistivity normal metal bilayer*. Beilstein J. Nanotechnol., vol. **11**, 858–865 (2020).

[20] Giazotto F., Heikkilä T. T., Luukanen A., Savin A. M., Pekola J. P. *Opportunities for mesoscopics in thermometry and refrigeration: Physics and applications*. Rev. Mod. Phys., vol. **78**, 217 (2006).

[21] Angers L., Chiodi F., Montambaux G., Ferrier M., Guéron S., Bouchiat H., Cuevas J. C. *Proximity dc squids in the long-junction limit*. Phys. Rev. B., vol. **77**, 165408 (2008).

[22] Courtois H., Meschke M., Peltonen J. T., Pekola J. P. *Origin of hysteresis in a proximity Josephson junction*. Phys. Rev. Lett., vol. **101**, 067002 (2008).

[23] Carillo F., Born D., Pellegrini V., Tafuri F., Biasiol G., Sorba L., Beltram F. *Relevant energy scale in hybrid mesoscopic Josephson junctions*. Phys. Rev. B, vol. **78**, 052506 (2008).

[24] García C. P., Giazotto F. *Josephson current in nanofabricated V/Cu/V mesoscopic junctions*. Appl. Phys. Lett., vol. **94**, 132508 (2009).

[25] Giazotto F., Peltonen J. T., Meschke M., Pekola J. P. *Superconducting quantum interference proximity transistor*. Nature Phys., vol. **6**, 254-259 (2010).

[26] Frielinghaus R., Batov I. E., Weides M., Kohlstedt H., Calarco R., Schäpers Th. *Josephson supercurrent in Nb/InN-nanowire/Nb junctions*. Appl. Phys. Lett., vol. **96**, 132504 (2010).

[27] Jung M., Noh H., Doh Y.-J., Song W., Chong Y., Choi M.-S., Yoo Y., Seo K., Kim N., Woo B.-C., Kim B., Kim J. *Superconducting junction of a single-crystalline Au nanowire for an ideal Josephson device*. ACS Nano, vol. **5**, 2271-2276 (2011).

[28] Golikova T. E., Hubler F., Beckmann D., Klenov N. V., Bakurskiy S. V., Kupriyanov M. Yu., Batov I. E., Ryazanov V. V. *Critical current in planar SNS Josephson junctions*. JETP Lett., vol. **96**, 668-673 (2012).

[29] Golikova T. E., Wolf M. J., Beckmann D., Batov I. E., Bobkova I. V., Bobkov A. M., Ryazanov, V. V. *Nonlocal supercurrent in mesoscopic multiterminal SNS Josephson junction in the low-temperature limit*. Phys. Rev. B, vol. **89**, 104507 (2014).

[30] Pekola J. P. *Towards quantum thermodynamics in electronic circuits*. Nature Phys., vol. **11**, 118-123 (2015).

[31] Paajaste J., Amado M., Roddaro S., Bergeret F. S., Ercolani D., Sorba L., Giazotto F. *Pb/InAs nanowire Josephson junction with high critical current and magnetic flux focusing*. Nano Lett., vol. **15**, 1803-1808 (2015).

[32] De Cecco A., Le Calvez K., Sacépé B., Winkelmann C. B., Courtois H. *Interplay between electron overheating and ac Josephson effect*. Phys. Rev. B, vol. **93**, 180505 (2016).

[33] Jabdaraghi R. N., Peltonen J. T., Saira O.-P., Pekola J. P. *Low-temperature characterization of Nb-Cu-Nb weak links with Ar ion-cleaned interfaces*. Appl. Phys. Lett., vol. **108**, 042604 (2016).

[34] Skryabina O. V., Egorov S. V., Goncharova A. S., Klimenko A. A., Kozlov S. N., Ryazanov V. V., Bakurskiy S. V., Kupriyanov M. Yu., Golubov A. A., Napolskii K. S., Stolyarov V. S. *Josephson coupling across a long single-crystalline Cu nanowire*. Appl. Phys. Lett., vol. **110**, 222605 (2017).

[35] Kim B.-K., Kim H.-S., Yang Y., Peng X., Yu D., Doh Y.-J. *Strong superconducting proximity effects in PbS semiconductor nanowires*. ACS Nano, vol. **11**, 221-226 (2017).

[36] Shishkin A. G., Skryabina O. V., Gurtovoi V. L., Dizhur S. E., Faley M. I., Golubov A. A., Stolyarov V. S. *Planar MoRe-based direct current nanoSQUID*. Supercond. Sci. Technol., vol. **33**, 065005 (2020).

[37] Zhang J., Jalil A. R., Tse P.-L., Kölzer J., Rosenbach D., Valencia H., Luysberg M., Mikulics M., Panaitov G., Grützmacher D., Hu Z., Lu J. G., Schäpers Th. *Proximity-Effect-Induced Superconductivity in Nb/Sb_2Te_3-Nanoribbon/Nb Junctions*. Ann. Phys., vol. **532**, 2000273 (2020).

[38] Murani A., Sengupta S., Kasumov A., Deblock R., Celle C., Simonato J. P., Bouchiat H., Guéron S. *Long-to short-junction crossover and field-reentrant critical current in Al/Ag-nanowires/Al Josephson junctions*. Phys. Rev. B, vol. **102**, 214506 (2020).

[39] Skryabina O. V., Bakurskiy S. V., Shishkin A. G., Klimenko A. A., Napolskii K. S., Klenov N. V., Soloviev I. I., Ryazanov V. V., Golubov A. A., Roditchev D., Kupriyanov M. Yu., Stolyarov V. S. *Environment-induced overheating phenomena in Au-nanowire based Josephson junctions*. Sci. Rep., vol. **11**, 15274 (2021).

[40] Golod T., Hovhannisyan R. A., Kapran O. M., Dremov V. V., Stolyarov V. S., Krasnov V. M. *Reconfigurable Josephson phase shifter*. Nano Lett., vol. **21**, 5240-5246 (2021).

[41] Sotnichuk S. V., Skryabina O. V., Shishkin A. G., Bakurskiy S. V., Kupriyanov M. Yu., Stolyarov V. S., Napolskii K. S. *Long Single Au Nanowires in Nb/Au/Nb Josephson Junctions: Implications for Superconducting Microelectronics*. ACS Applied Nano Materials, vol. **11**, 17059-17066 (2022).

[42] Babich I., Kudriashov A., Baranov D., Stolyarov V. S. *Limitations of the Current–Phase Relation Measurements by an Asymmetric dc-SQUID*. Nano Lett., vol. **23**, 6713-6719 (2023).

[43] Edwards J. T., Thouless D. J. *Numerical studies of localization in disordered systems*. J. Phys. C: Solid State Phys., vol. **5**, 807 (1972).

[44] Thouless D. J. *Maximum Metallic Resistance in Thin Wires*. Phys. Rev. Lett., vol. **39**, 1167–1169 (1977).

[45] Thouless D. J. *Electrons in disordered systems and the theory of localization*. Phys. Rep., vol. **13**, 93-142 (1974).

[46] Altland A., Gefen Y., Montambaux G. *What is the Thouless Energy for Ballistic Systems?* Phys. Rev. Lett., vol. **76**, 1130-1133 (1996).

[47] Usadel K. D. *Generalized diffusion equation for superconducting alloys*. Phys. Rev. Lett., vol. **25**, 507 (1970).

[48] Golubov A. A., Kupriyanov M. Y., Siegel, M. *Density of states anomalies in hybrid superconductor-ferromagnet-normal metal structures*. JETP Lett., vol. **81**, 180-184 (2005).

[49] Likharev K. K., Iakobson L. A. *Steady-state properties of superconducting bridges*. Sov. Phys. – Tech. Phys., vol. **20**, 950 (1975).

[50] Kupriyanov M. Yu., Lukichev V. F. *The influence of the proximity effect in the electrodes on the stationary properties of S–N–S Josephson structures*. Sov. J. Low Temp. Phys., vol. **8**, 526-529 (1982).

[51] Fabrication process details along with the full experimantal data for these series of the junctions will be publushed elsewhere soon.

[52] Kupriyanov M. Yu., Lukichev V. F., Orlikovskii A. A. *Stationary properties of quasi-two-dimensional josephson weak links*. Sov. Microelectronics, vol. **15**, 185-189 (1986).

[53] Baryshev Y. P., Vasil'ev A. G., Dmitriyev A. A., Kupriyanov M. Y., Lukichev V. F., Luk'yanova I. Y., Sokolova I. S. *Theoretical and experimental study of the josephson effect in submicron SN-N-NS structures*. Lithography in microelectronics, vol. **8**, 187-197 (1989).

[54] Bosboom V., Van der Vegt J. J. W., Kupriyanov M. Yu., Golubov A. A. *Selfconsistent 3D model of SN-N-NS Josephson junctions*. Supercond. Sci. Technol., vol. **34**, 115022 (2021).